Journal of the European Ceramic Society 22 (2002) 761–768

www.elsevier.com/locate/jeurceramsoc

Mullite–molybdenum composites fabricated by pulse electric current sintering technique

R. Sivakumar*, D. Doni Jayaseelan, T. Nishikawa, S. Honda, H. Awaji

Department of Materials Science and Engineering, Nagoya Institute of Technology, Gokiso-cho, Showa-ku, Nagoya 466 8555, Japan

Received 7 March 2001; accepted 29 May 2001

Abstract

Pulse electric current sintering of monolithic mullite and mullite/0–100 vol.% Mo composites was performed in vacuum of 4.5×10^{-5} Torr at temperatures and pressures of 1500 °C and 20 MPa, respectively. No traces of additional phases were observed by SEM and XRD for these composites. Microstructural observations reveal that Mo (molybdenum) particles dispersed uniformly at lower Mo contents and exhibited flaky and elongated structure at higher content. Simultaneous increase of fracture strength and toughness occurred with increase in Mo content. It attained a maximum of 1.1 GPa and 9.2 MPa $m^{1/2}$, respectively for 90 vol.% Mo composites. The increase in flexural strength is due to smaller initial flaws in mullite/Mo composites for lower Mo contents and due to plastic deformation of Mo phase for higher Mo contents. Similarly, frontal process zone toughening and crack bridging are expected to be the responsible mechanisms for enhanced toughness in these composites. Partial debonding in the mullite–Mo interface, giving rise to plastic deformation of Mo phase also contributes in the increase of toughness values.

Keywords: Microstructure-final; Mo; Mullite; PECS technique; Sintering; Strength; Toughness and toughening

1. Introduction

Brittle ceramic materials subjected to mechanical stress, show only little resistance for the propagation of crack and fail catastrophically. Thus, they have less potential to be utilized in the structural applications. The mechanical properties of these materials can be increased by incorporation of secondary phases such as particulates,[1,2] platelets,[3,4] fibres[5] and whiskers.[6] Recently, Nawa et al.[7] have reported significant results of the developed bending strength of 2.1 GPa and fracture toughness as high as 11.4 MPa $m^{1/2}$ in 3Y-TZP/Mo nanocomposites. This improvement of mechanical properties is due to the presence of nano-sized particles in the matrix grains denominated "intra-type nanocomposites" by Niihara.[8]

Regarding the toughening mechanisms of the polycrystalline ceramics, we have classified them into three categories.[9] They are (i) the frontal process zone toughening mechanism related to the intrinsic fracture energy of the material, which creates the damaged zone in front of the crack tip. In this toughening mechanism, the increase in size of frontal process zone enhances the intrinsic fracture toughness of the material. The toughening in nanocomposites proposed by Niihara[8] is based on this mechanism. (ii) The crack bridging mechanism acting in the wake region of the process zone related to the extrinsic increase in the toughness, due to the reduction of the stress intensity factor at the crack tip. The toughening in ceramic matrix composites with relatively large secondary phase inclusions[10–15] is associated with this mechanism. (iii) The macroscopic crack deflection mechanism attributed to the decrease in energy-release rate and thus increasing the stress intensity factor at the crack tip. Clegg et al.[16,17] designed a tough multilayer SiC with a weak graphite interface, which deflects the crack propagation. Multilayered structures of combination of tough/weak materials,[18,19] and structure-controlled self-reinforced composites[20] have this crack deflection mechanism.

In this study, we have focussed our attention on the fabrication of ceramic matrix composites reinforced with ductile inclusions and metal matrix composites reinforced with brittle inclusions. Significant works have been made by us in recent years to understand the crack

* Corresponding author. Tel.: +81-52-735-5287; fax: +81-52-735-5294.

E-mail address: sivachi@mse.nitech.ac.jp (R. Sivakumar).

0955-2219/02/$ - see front matter
PII: S0955-2219(01)00375-2

growth resistance and strength behaviour of ceramic/metal composites.[21–23] Molybdenum (Mo) was reinforced with the mullite matrix composite because they have similar thermal expansion coefficients at room temperature in which the thermal residual stresses reduce due to the minimum thermal expansion mismatch. In addition, Mo has a high melting point (2610 °C) and good sinterability at low temperatures (1400 °C).[24] Thus, the mullite/Mo system is effectively used in the fabrication of functionally gradient materials.[25,26] Addition of a small quantity of sintering aid is the most effective way to achieve full densities and to avoid the abnormal grain growth of mullite[27–30]. MgO was used in small quantity (0.25 wt% of mullite content) to promote the densification of these composites.

A new sintering method widely known as the pulse electric current sintering (PECS) technique was used for sintering mullite/Mo composites. PECS technique is used to sinter a wide range of materials fast and fully dense. This paper emphasis the microstructural features of mullite/Mo composites with increasing Mo content from 0 to 100% in connection with their toughening mechanisms and fracture behaviour.

2. Experimental procedure

2.1. Materials preparation

Starting materials used to prepare the powder mix are as follows: mullite (Kyoritsu Yogyo Co., KM102) having an average particle size of 1.3 μm and molybdenum (Mitsuwa's Pure Chemical Co.) having an average particle size of 2.7 μm. Mo of various compositions ranging from 0 to 100 vol.% was added to mullite. MgO was added as the sintering aid to the mixed powder for better densification. The mixture was prepared by mixing the starting materials in the polyethylene pot with ethanol for 24 h. Each slurry was dried at 110 °C for 24 h. It was then ground in the high purity alumina mortar and passed through a screen of 350 μm in size.

2.2. Pulse electric current sintering

SPS-515S apparatus (Sumitomo Coal Mining Co., Ltd.) was used for sintering the monolithic mullite and the composite specimens. The graphite die used for the sintering purpose had the dimensions of outer and inner diameter of 40 and 20 mm, respectively with a pair of graphite punches on both sides of the die. To ensure the good electrical contact, a graphite foil was introduced between the punches and die. The graphite die was carefully covered with ceramic wool for thermal insulation. The sieved powder mix was packed in the die and sintered in vacuum with a heating rate of 150 °C/min up to 1500 °C. An increased pressure of 20 MPa was given simultaneously to the punches during sintering. The specimens were held for 10 min at the maximum temperature where there was no shrinkage. Then, the temperature was slowly reduced to room temperature. An optical pyrometer was used to monitor the temperature of the specimen, which was focussed to the die surface. Sintered specimens had the dimensions of 20 mm diameter and 10 mm thickness, approximately.

2.3. Sintering mechanism

Pulse electric current sintering is a newer technique, similar to hot pressing, which is carried out in a graphite die. Pulsed d.c. current is applied instantaneously through the electrodes to top and bottom punches of graphite die along with the pressure. The low heat capacity of the graphite die allows rapid heating and cooling, thus promoting heat and mass transfer.

Main effects for enhancement of sintering in the hot pressing process are the thermal diffusion and plastic flow of particles due to high pressure, whereas in this PECS technique, the spark discharge occurs at the contact between particles of material. Thus, a local high temperature is generated momentarily. This causes evaporation and melting on the surface of the powder particles and necking is formed around the area of contact between the particles, hence sintering the material.

2.4. Characterization

Sintered densities were obtained by using Archimedes method with distilled water as the medium. Phase identification of the specimens was carried out by X-ray diffraction (XRD) analysis using Cu-K_α radiation for the polished surface of specimens. The microstructure analysis of the fractured surfaces and the crack propagation behaviour in the polished surface were observed by a scanning electron microscope (SEM).

2.5. Mechanical properties

An elastic modulus of each composite was measured by an ultrasonic method using a disk specimen as sintered. Then, the specimens were machined with a diamond wheel to the dimension of $2\times2\times10$ mm^3. The tensile surface was polished down with a diamond slurry of abrasive size 3 μm for the flexural strength test and beveling was carried out to the tensile edges. The fracture strength was evaluated by a three-point flexural testing at room temperature with a cross-head speed of 0.1 mm/min and a lower span of 8 mm. Hardness was measured for the polished specimens using Vickers indenter. A load of 98 and 196 N was applied for a period of 15 s to the monolithic mullite and composite specimens. Simultaneously, the fracture toughness was also measured by the indentation fracture (IF) method with Vickers hardness tester

by indenting on the polished surface of the specimens. The fracture toughness was calculated from the following equation of JIS R1607 standards,

$$K_{Ic} = (0.026E^{0.5}P^{0.5}a)/c^{1.5} \quad (1)$$

where E is Young's modulus, P the load applied for indentation, a dimension of the indentation and c crack length measured from the center of the contact pattern. The fracture toughness was also estimated by the single edge V notch beam (SEVNB) method. The V-notch was formed by a diamond slicing wheel developed by Awaji et al.[31,32] A three-point bending strength test was undergone for V-notched specimens under mode I loading and fracture toughness was evaluated by the following equation of JIS R1607 standards,

$$K_{Ic} = \left(\frac{PS}{B\bar{w}^{3/2}}\right)\left\{\frac{3}{2}\left(\frac{C}{\bar{w}}\right)^{1/2} Y\left(\frac{C}{\bar{w}}\right)\right\} \quad (2)$$

and

$$Y\left(\frac{C}{\bar{w}}\right) = \frac{\left[1.99 - \frac{C}{\bar{w}}\left(1-\frac{C}{\bar{w}}\right)\left\{2.15 - 3.93\frac{C}{\bar{w}} + 2.7\left(\frac{C}{\bar{w}}\right)^2\right\}\right]}{\left(1+2\frac{C}{\bar{w}}\right)\left(1-\frac{C}{\bar{w}}\right)^{3/2}} \quad (3)$$

where, S is span length of the three-point flexure test, B thickness and $\bar{w}$width of the specimen. Eq. (3) is applied for $\frac{S}{\bar{w}} = 4$ and $0 \leqslant \frac{C}{\bar{w}} \leqslant 1$.

3. Results and discussion

3.1. Densification and phases

The variation of relative densities with Mo content is shown in Fig. 1. It is seen that the densities of the composites are more than 98% of theoretical densities, where the theoretical densities of mullite and Mo are assumed to be 3.17×10^3 and 10.22×10^3 kg/m^3, respectively. These results indicate that both monoliths and mullite/Mo composites were well sintered at 1500 °C in vacuum.

The phases in the mullite/Mo composites were determined at room temperature by XRD analysis. This analysis revealed that the composites are composed of pure mullite and Mo phases and no new phases are formed during sintering.

3.2. Microstructures

The typical electron micrographs of Mo reinforced mullite matrix composites showing the polished surfaces with increasing Mo content are shown in Fig. 2. At lower Mo concentrations, Mo particles have a uniform dispersion in the mullite matrix. While, at 30 vol.% Mo, elongated and flaky shaped metal ligaments were formed. At even higher Mo contents such as 50 vol.% Mo, the flaky Mo are well interlinked to form a network structure. These interconnected Mo structures are accompanied with the significant increase in the toughness of mullite–Mo composites by increasing the frontal process zone area

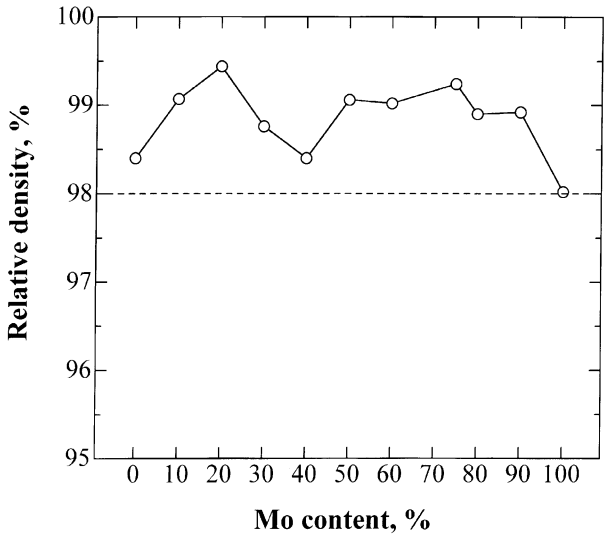

Fig. 1. Variation of densities of mullite–Mo composites with Mo content sintered at 1500 °C.

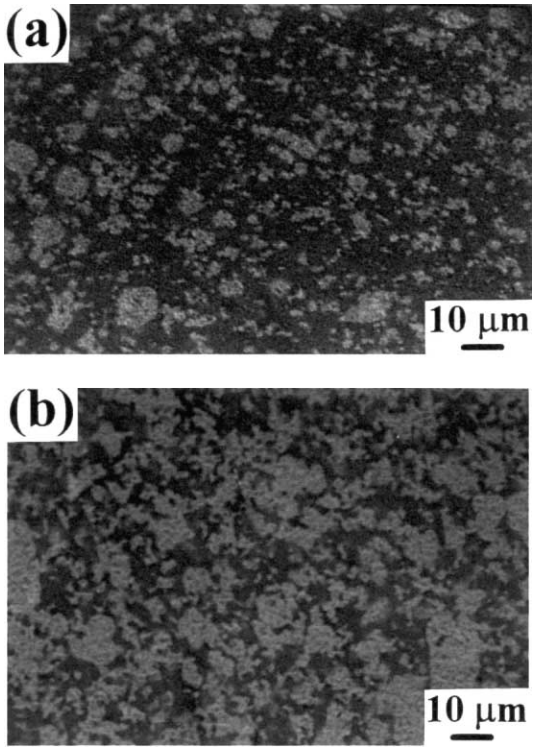

Fig. 2. Micrographs of polished surface of mullite-Mo composites sintered at 1500 °C with (a) 30 vol.% Mo and (b) 50 vol.% Mo.

and therefore resisting the crack propagation, which is characterized for metal matrix composites (the frontal process zone toughening mechanism).

The microstructural investigation of the fracture surfaces (Fig. 3) reveals features which correlate the strengthening and toughening of mullite/Mo composites with various Mo content. From the fractured surfaces, it is seen that many Mo grains are situated in the grain boundaries of mullite matrix at lower Mo content, which is substantially pinning the grain growth of mullite grains. Thus, the

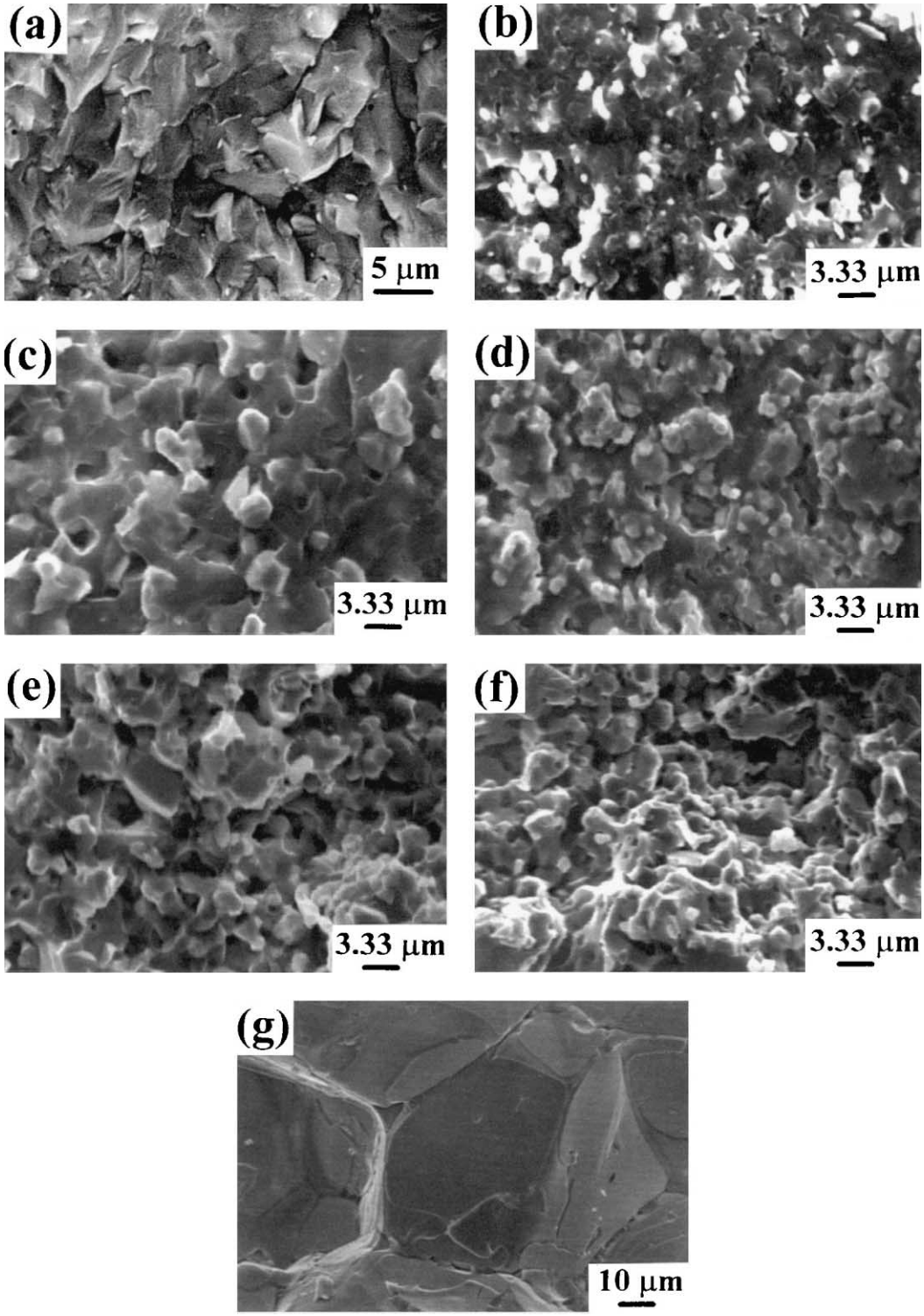

Fig. 3. Micrographs of fractured surface of monolithic and mullite-Mo composites sintered at 1500 °C. (a) Mullite; (b) 20 vol.% Mo; (c) 40 vol.% Mo; (d) 60 vol.% Mo; (e) 75 vol.% Mo; (f) 90 vol.% Mo; (g) molybdenum.

strength of the composites increased substantially. It is also observed that the fracture is mainly transgranular mode for composites with even lower Mo content. This may be due to the strengthening of grain boundaries of the matrix by reduction of residual stresses on the interfaces. Anisotropic thermal expansions caused by cooling monolithic mullite may generate residual stresses on the interface.[33] The presence of Mo metal ligaments between mullite grains and/or inside mullite grains release the residual stresses on interfaces of mullite grains.

Cavities resulting from the pullouts of Mo particles are found in the fractured surfaces of lower Mo content composites due to weaker interfacial bonding strength between the interfaces of ductile Mo phase and brittle mullite matrix. This interfacial bonding strength has a direct dependence on the extent of debonding. The partial debonding of the interface results in larger crack opening displacements (COD) upon ductile phase rupture, hence high toughness which relates to the crack bridging mechanism. But, due to the spherical geometry and small gauge length of the Mo particles, the degree of partial debonding is poor in particulate reinforced composites tending to complete interfacial debonding.[10,11] Thus, it limits the plastic deformation of Mo particles and there is almost no contribution to increase in toughness. It is, hence, required to have a strong interfacial bond between the matrix and ductile phases.

For higher Mo content, the network structure of Mo particles is formed, therefore, increasing the gauge length of the metal phase.[34–36] In the case of the metal having larger gauge lengths, even if the interfacial bond strength is lower, it is difficult to pull out the brittle mullite particles leading to the extensive plastic deformation of ductile Mo matrix, thus improving the toughness of these composites.

3.3. Mechanical properties

A plot of Young's modulus (E) as a function of Mo content in the mullite/Mo composites is shown in Fig. 4. As expected, the values of elastic moduli increase with the Mo content, because Mo has higher elastic moduli than of mullite. The solid lines represent the upper and the lower bounds of predicted elastic moduli procured using Voigt and Reuss models for the composite materials composed of mullite and molybdenum. The predicted elastic moduli of these composites were calculated using the values of 220 GPa for mullite and 325 GPa for molybdenum respectively. The experimentally obtained values are shown by the dotted lines. Comparing the experimental and the predicted values, it is seen that the experimental data are very close with the lower bound of Reuss model. This may be due to poor interfacial bonding strength between the matrix and secondary phase reinforcing particulates that is confirmed by the fractured surfaces of composites (Fig. 3).

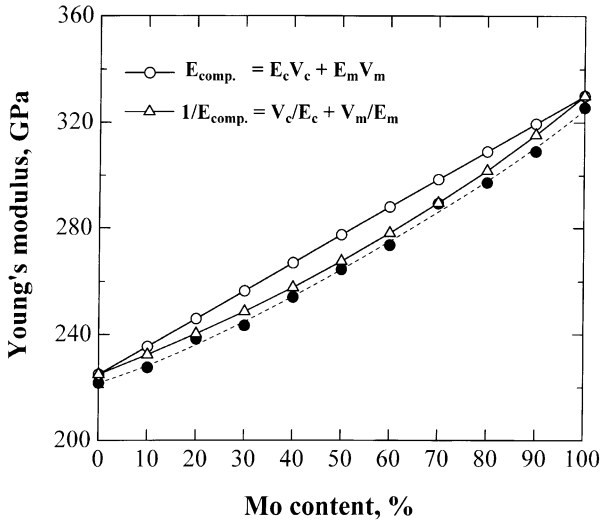

Fig. 4. Dependence of Young's modulus on the Mo content for mullite–Mo composites.

The hardness of mullite/Mo composites as it varied with the Mo content is plotted in the Fig. 5. The hardness of monolith mullite and Mo is 13 and 2.1 GPa, respectively. Since the hardness of the Mo phase is lower than that of mullite, the hardness of the mullite/Mo composites as a whole decreases with the increase in Mo content. The Vickers hardness values predicted by the Voigt and Reuss models are represented by the solid lines. The experimental values of hardness represented by dashed lines lie in between the upper and lower bounds of Voigt and Reuss adhering the predicted hardness values.

The dependence of bending strength with the Mo content is shown in Fig. 6. The fracture strength increased gradually with Mo content. It attained a maximum value of 1.1 GPa at 90 vol.% Mo from 441

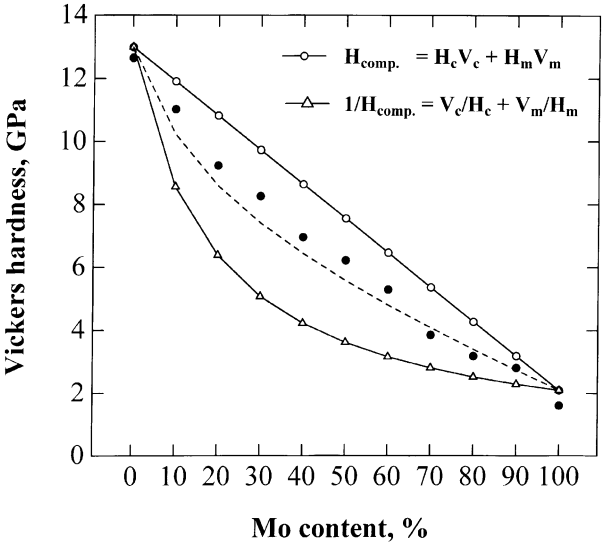

Fig. 5. Dependence of Vickers hardness on the Mo content for mullite–Mo composites.

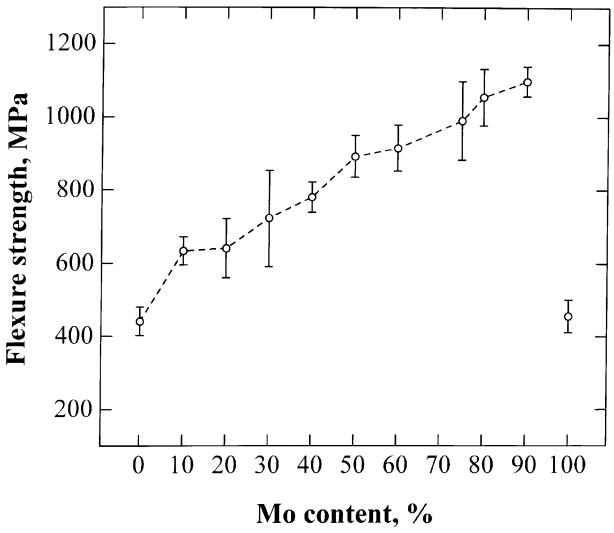

Fig. 6. Dependence of flexure strength on the Mo content for mullite–Mo composites.

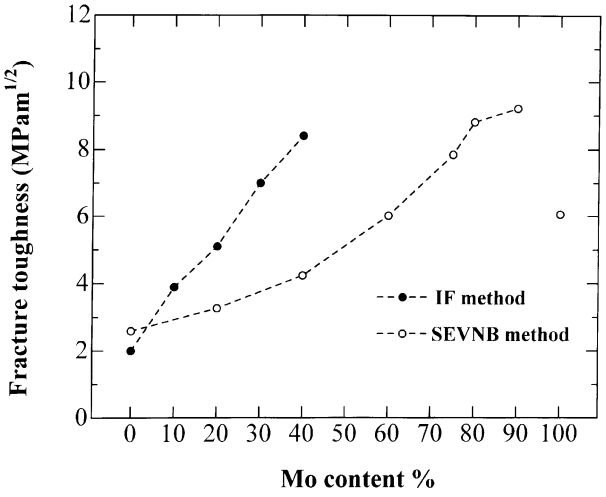

Fig. 7. Dependence of fracture toughness on the Mo content for mullite–Mo composites determined by the IF and SEVNB methods.

MPa for monolithic mullite. The strengthening of lower Mo content composites is attributed to smaller mullite grains due to the dispersion of ductile secondary phase that limit the initial flaw sizes. The sintering aid (MgO) in a smaller amount also contributes in increased strength of these composites.[21] That is, the sintering aid disperses Mo particulates uniformly avoiding Mo agglomerates in the mullite matrix, in turn increasing flexural strength. Similarly, for the higher Mo content composites, the increase in strength can be explained by plastic deformation of Mo matrix and also may be due to pinning of mullite grains in the grain boundaries of Mo. The gradual increase in strength from lower to higher Mo contents had a sudden deterioration for the pure Mo monolithics. This may be due to the increased grain size of Mo. The sintered Mo grains had a size of more than 10 times that of the starting grain size.

The variation of fracture toughness with the concentration of Mo added to the mullite matrix was evaluated by the IF method. Up to 40 vol.% Mo, there was a steep increase in the toughness values (Fig. 7). Composites with more than 50 vol.% Mo had a very high toughness so that there was no crack propagation after the Vickers indentation. Calculation of the fracture toughness was carried out utilizing Eq. (1) where the calibration constant is 0.026 according to JIS R1607 standards. This constant is suitable only for the brittle structural ceramics and not for metal reinforced ceramics. Hence, the IF method tended to overestimate the fracture toughness of the tested specimens. A SEVNB (single edge V-notch beam) method proposed by Awaji et al.[31] was then considered to evaluate the fracture toughness of these composites precisely. The V-shaped notch introduced by specially designed diamond slicing wheel had a very sharp root radius of around 10 μm with the notch angle below 30°. The fracture toughness values evaluated by the SEVNB method increased gradually and reached a maximum value of 9.2 MPa $m^{1/2}$ with 72% increase than the pure mullite.

For the monolith molybdenum, the fracture toughness had a decreased value of 6.1 MPa $m^{1/2}$. The cardinal effect in decrease of toughness values can be explained due to the contribution of failure mode observed after the flexural tests. Intergranular mode of fracture was observed for Mo monolithic specimens as in Fig. 3. The most common in metallic materials is the segregation of impurities or solute elements which alter the local bonding so as to reduce the cohesive strength across the interface.[36] Due to the segregation of impurities, the energy at the grain boundaries gets lowered to produce faceted morphologies.[37] The complete lack of plastic deformation of Mo grains facilitating the intergranular failure, reduced the fracture toughness values.

The crack propagation behaviour at lower Mo content was analyzed to investigate the mechanisms responsible for enhanced fracture toughness of the mullite/Mo composites than that of monolith mullite. The toughening mechanisms expected in these composites may be frontal process zone toughening and crack bridging. The nano-toughening proposed by Niihara will also be expected since the starting materials had the grain size of more than 1 μm while the frontal process zone size for the structural ceramics is about 10 μm.[8] Direct microscopic evidence is presented in support of the explanation of bridging mechanism in an indented surface as shown in Fig. 8. The lower the molybdenum content in matrix, smaller is the deviation of crack propagation (Fig. 8a). The particulates coalesced and had an elongated structure at higher Mo concentration, which were formed due to the necking of particles. Thus, the advancing crack tip is progressively impeded and bridged by the elongated particles, subsequently increasing the fracture toughness values (Fig. 8b).

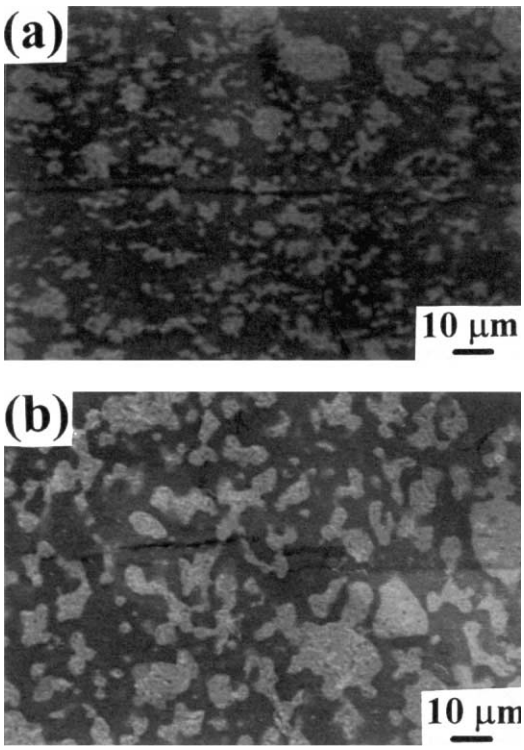

Fig. 8. Micrographs of crack propagation behavior for mullite–Mo composites sintered at 1500 °C with (a) 20 vol.% Mo and (b) 30 vol.% Mo.

4. Conclusions

1. Monolithic mullite and mullite/Mo composites were fabricated by PECS technique at 1500 °C, in a vacuum of 4.5×10^{-5} Torr. Composites were prepared varying the Mo contents from 0 to 100 vol.%. The bulk densities of the sintered materials were more than 98% of theoretical densities.

2. Mullite/Mo composites were composed of pure mullite and Mo phases. No oxides of Mo were formed during sintering which is confirmed by XRD analysis.

3. Mo particles had a uniform dispersion in the mullite matrix at lower contents. Elongated and flaky Mo was formed at 30 vol.% Mo and at higher volume contents such as 50 vol.%, interconnected Mo structures were formed.

4. Even at lower Mo content, the change in the failure mode from intergranular to transgranular mode of fracture was observed and thus increased the toughness of the composites.

5. At lower Mo content composites, the increase of strength was due to small mullite grains with smaller critical flaw sizes. Similarly for higher Mo content composites, the increase in strength is mainly due to plastic deformation of ductile Mo matrix and also may be due to pinning of mullite grains present in grain boundaries of molybdenum.

6. The toughening mechanisms expected in these composites are frontal process zone toughening and crack bridging mechanisms. The pullouts of ductile Mo particles from the mullite matrix of lower Mo content composites also increase the extrinsic fracture toughness.

7. Significant enhancement of fracture strength and toughness were observed and attained a maximum value of 1.1 GPa and 9.2 MPa $m^{1/2}$, respectively for mullite/Mo composite of 90 vol.% Mo.

8. The decrease in strength of pure Mo is purely ascribed to larger grain size, which is more than 10 times that of initial grain size. Its decrease of toughness is due to intergranular mode of fracture formed and/or the segregation of impurities in the grain boundaries.

References

1. Garcia, D. E., Schicker, S., Bruhn, J., Janssen, R. and Claussen, N., Processing and mechanical properties of pressureless sintered Nb–Al_2O_3-matrix composites. *J. Am. Ceram. Soc.*, 1998, **81**(2), 429–433.
2. Wadsworth, I. and Stevens, R., Strengthening and toughening of cordierite by the addition of silicon carbide whiskers, platelets and particles. *J. Mater. Sci.*, 1991, **26**, 6800–6808.
3. Rezaie, H. R., Rainforth, W. M. and Lee, W. E., Fabrication and mechanical properties of SiC platelet reinforced mullite matrix composites. *J. Eur. Ceram. Soc.*, 1999, **19**, 1777–1787.
4. Nischik, C., Seibold, M. M., Travitzky, N. A. and Claussen, N., Effect of processing on mechanical properties of platelet reinforced mullite composites. *J. Am. Ceram. Soc.*, 1991, **74**(10), 2464–2468.
5. Kerans, R. J., Hay, R. S. and Pagano, N. J., The role of the fibre-matrix interface in ceramic composites. *Am. Ceram. Soc. Bull.*, 1989, **8**(2), 429–442.
6. Ruh, R. and Mazdiyashi, K. S., Mechanical and microstructural characterization of mullite and mullite–SiC whisker and ZrO2-toughened-mullite-SiC whisker composite. *J. Am. Ceram. Soc.*, 1988, **71**, 503–512.
7. Nawa, M., Yamazaki, K., Sekino, T. and Niihara, K., Microstructure and mechanical behaviour of 3Y-TZP/Mo nanocomposites possessing a novel interpenetrated intragranular microstructure. *J. Mater. Sci.*, 1996, **31**, 2849–2858.
8. Niihara, K., New design concept of structural ceramics-ceramic nanocomposites. *J. Ceram. Soc. Jpn*, 1991, **99**(10), 974–982.
9. Awaji, H., Choi, S.-M., Ebisudani, T. and Jayaseelan, D. D., Toughening mechanisms of Structural Ceramics (in Japanese). *J. Ceram. Soc. Jpn*, 2000, **108**(6), 611–613.
10. Sun, X. and Yeomans, J., Microstructure and fracture toughness of nickel particle toughened alumina matrix composites. *J. Mater. Sci.*, 1996, **31**, 875–880.
11. Sun, X. and Yeomans, J., Optimization of a ductile particle toughened ceramics. *J. Am. Ceram. Soc.*, 1996, **79**(10), 2701–2717.
12. Schicker, S., Erny, T., Garcia, D. E., Janssen, R. and Claussen, N., Microstructure and mechanical properties of Al-assisted Fe/Al_2O_3 cermets. *J. Eur. Ceram. Soc.*, 1999, **19**, 2455–2463.
13. Flinn, B. D., Ruhle, M. and Evans, A. G., Toughening in composites of Al_2O_3 reinforced with Al. *Acta. Metall.*, 1989, **37**(11), 3001–3006.
14. Raddatz, O., Schneider, G. A., Mackens, W., Vob, H. and Claussen, N., Bridging stresses and R-curves in ceramic/metal composites. *J. Eur. Ceram. Soc.*, 2000, **20**, 2261–2273.

15. Prielipp, H., Knechtel, M., Claussen, N., Streiffer, S. K., Mullejans, H., Ruhle, M. and Rodel, J., Strength and fracture toughness of aluminium/alumina composites with interpenetrating networks. *Mater. Sci. Eng*., 1995, **A197**, 19–30.
16. Clegg, W. J., Kendall, K., McN, N., Alford Button, T. W. and Birchall, J. D., A simple way to make tough ceramics. *Nature*, 1990, **347**, 455–457.
17. Clegg, W. J., The fabrication and failure of laminar ceramic composites. *Acta Metall. Mater*., 1992, **40**(11), 3085–3093.
18. Liu, H. and Hsu, S. M., Fracture behaviour of multilayer Silicon nitride/Boron nitride ceramics. *J. Am. Ceram. Soc*., 1996, **79**(9), 2452–2457.
19. Kovar, D., Thouless, M. D. and Halloran, J. W., Crack deflection and propagation in layered silicon nitride/Boron nitride ceramics. *J. Am. Ceram. Soc*., 1998, **81**(4), 1004–1012.
20. Hirao, K., Ohashi, M., Brito, M. E. and Kanzaki, S., Processing strategy for producing highly anisotropic silicon nitride. *J. Am. Ceram. Soc*., 1995, **78**(6), 1687–1690.
21. Sivakumar, R., Doni Jayaseelan, D., Nishikawa, T., Honda, S. and Awaji, H., Influence of MgO on microstructure and properties of mullite/Mo composites fabricated by pulse electric current sintering. *Ceram. Int*. (in press).
22. Amutharani, D., Doni Jayaseelan, D., Nishikawa, T. and Awaji, H., Pressureless sintering of mullite/Mo composites. *J. Ceram. Soc. Jpn*. (Submitted).
23. Doni Jayaseelan, D., Honda, S., Nishikawa, T. and Awaji, H., Fabrication and characterization of mullite/Mo composites by pulse electric current sintering (PECS) technique. In *Proceedings of 16th Japan–Korea International Ceramics Seminar, Japan,* 1999, pp. 88–92.
24. Khan, A. A. and Labbe, J. C., Aluminium nitride-molybdenum ceramic matrix composites. Influence of molybdenum addition on electrical, mechanical and thermal properties. *J. Eur. Ceram. Soc*., 1997, **17**, 1885–1890.
25. Sivakumar, R., Takenaka, H., Honda, S., Nishikawa, T. and Awaji, H., Temperature distributions in a stress-relief type hollow cylinder of functionally graded materials under thermal shock. In *Proceedings of 16th Japan–Korea International Ceramic Seminar, Japan,* 1999, pp. 324–328.
26. Tomsia, A. P., Saiz, E., Ishibashi, H., Diaz, M., Requena, J. and Moya, J. S., Powder processing of mullite/Mo functionally graded materials. *J. Eur. Ceram. Soc*., 1998, **18**, 1365–1371.
27. Bai, S. I. and Baik, S., Critical concentration of MgO for the prevention of abnormal grain growth in Alumina. *J. Am. Ceram. Soc*., 1994, **77**(10), 2499–2504.
28. Montanaro, L., Perrot, C., Esnouf, C., Thollet, G., Fantozzi, G. and Negro, A., Sintering of industrial mullites in the presence of magnesia as a sintering aid. *J. Am. Ceram. Soc*., 2000, **83**(1), 189–196.
29. Heuer, A. H., The role of MgO in the sintering of alumina. *J. Am. Ceram. Soc*., 1979, **62**(5-6), 317–318.
30. Bennison, S. J. and Harmer, P., Effect of MgO solute on the kinetics of grain growth in Al_2O_3. *J. Am. Ceram. Soc*., 1983, **66**(5), C90–C92.
31. Awaji, H. and Sakaida, Y., V-notch technique for single edge notched beam and chevron notch methods. *J. Am. Ceram. Soc*., 1990, **73**(11), 3522–3523.
32. Awaji, H., Watanabe, T. and Sakaida, Y., Fracture toughness measurements of ceramics by V-notch technique. *Ceram. Int*., 1992, **18**, 11–17.
33. Green, D. J., *An Introduction to the Mechanical Properties of Ceramics*. Cambridge University Press, Cambridge, 1998 pp. 38.
34. Tuan, W. H., Lin, I. C., Pai, Y. P. and Chang, S. T., Toughening Al_2O_3 with NiAl and NiAl(Fe) particles. *Br. Ceram. Trans*., 2000, **99**(2), 88–91.
35. Ashby, A. F., Blunt, F. J. and Bannister, M., Flow Characteristics of Highly constrained metal wires. *Acta Metall*., 1989, **37**, 1847–1857.
36. Chang, L., Chen, S. C., Tuan, W. H. and Brook, R. J., *J. Eur. Ceram. Soc*., 1993, **12**, 479–485.
37. Chell, G. G., *Developments in Fracture Mechanics—2*. Applied Science Publishers, London and New Jersey, 1981 pp. 200–203.